ÉCOLE POLYTECHNIQUE FÉDÉRALE DE LAUSANNE

MATHICSE

Mathematics Institute of Computational Science and Engineering

School of Basic Sciences - Section of Mathematics

MATHICSE Technical Report

Nr. 16.2015

June 2015

A fluid-structure interaction algorithm using radial basis function interpolation between non-conforming interfaces

Simone Deparis, Davide Forti, Alfio Quarteroni

http://mathicse.epfl.ch

Phone: +41 21 69 37648

Address:
EPFL - SB - MATHICSE (Bâtiment MA)
Station 8 - CH-1015 - Lausanne - Switzerland

Fax: +41 21 69 32545

A fluid–structure interaction algorithm using radial basis function interpolation between non-conforming interfaces

Simone Deparis, Davide Forti and Alfio Quarteroni

Abstract We consider a fluid-structure interaction (FSI) problem discretized by finite elements featuring two different grids that do not necessarily agree on the interface separating the computational domain of the fluid from the one of the structure. After identifying a master domain (the structural domain) and a slave domain (the fluid domain), we build up two Radial Basis Function (RBF) inter-grid operators, one Π_{fs} from master to slave, and the other Π_{sf} from slave to master. Then, we enforce the kinematic condition by equating the fluid velocity at the interface as the image through Π_{fs} of the temporal derivative of the structural displacement. On the other hand, the dynamic interface condition is fulfilled via a variational method where the strong form of the structural normal stress is obtained as the image through Π_{sf} of the strong form of the fluid normal stress. A numerical verification is carried out for a straight cylinder and for a patient-specific arterial bypass geometry. This new method is easy to implement and optimally accurate.

1 Introduction and Model Description

In this paper we propose a new method for the coupling of an FSI problem featuring two finite element grids that are non-conforming at the interface separating the computational fluid domain Ω^f from the computational structure domain Ω^s. This method is based on a suitable way to enforce the kinematic condition and (the strong form of) the dynamic condition via the use of two distinct RBF interpolation

Simone Deparis, e-mail: simone.deparis@epfl.ch
EPFL – École Polytechnique Fédérale de Lausanne, Station 8, Lausanne, CH–1015, Switzerland

Davide Forti, e-mail: davide.forti@epfl.ch
EPFL – École Polytechnique Fédérale de Lausanne, Station 8, Lausanne, CH–1015, Switzerland

Alfio Quarteroni, e-mail: alfio.quarteroni@epfl.ch
EPFL – École Polytechnique Fédérale de Lausanne, Station 8, Lausanne, CH–1015, Switzerland
MOX - Politecnico di Milano, via Bonardi 9, Milano, 20133, Italy (on leave)

operators, one from Ω^f to Ω^s and the others from Ω^s to Ω^f. In our FSI model, the incompressible Navier–Stokes equations are written in ALE coordinates, whereas the linear elasticity model for the structure in a Lagrangian frame of reference. A third field, the so–called geometry problem, allows to determine the displacement $\mathbf{d}_f$ of the fluid domain which defines, in turn, the ALE map. In this paper we compute $\mathbf{d}_f$ as the harmonic extension of the trace of the solid displacement $\hat{\mathbf{d}}_s$ at the reference fluid structure interface $\hat{\Gamma}$, to the fluid reference domain $\hat{\Omega}^f \subset \mathbb{R}^3$:

$$-\Delta \hat{\mathbf{d}}_f = 0 \text{ in } \hat{\Omega}^f, \quad \hat{\mathbf{d}}_f = \hat{\mathbf{d}}_s \text{ on } \hat{\Gamma}, \tag{1}$$

complemented with boundary conditions on $\partial\hat{\Omega}^f \setminus \hat{\Gamma}$. The solution of the geometry problem $\hat{\mathbf{d}}_f$ defines the ALE map $\mathscr{A}_t(\hat{\mathbf{x}}) = \hat{\mathbf{x}} + \hat{\mathbf{d}}_f(\hat{\mathbf{x}},t)\ \forall \hat{\mathbf{x}} \in \hat{\Omega}^f$, and consequently the current fluid domain configuration at time t

$$\Omega_t^f = \{\mathbf{x} = \mathscr{A}_t(\hat{\mathbf{x}}) |\ \hat{\mathbf{x}} \in \hat{\Omega}^f\}.$$

The Navier–Stokes equations written in ALE coordinates read:

$$\rho_f \left.\frac{\partial \mathbf{u}_f}{\partial t}\right|_{\hat{\mathbf{x}}} + \rho_f((\mathbf{u}_f - \mathbf{w})\cdot\nabla)\mathbf{u}_f - \nabla\cdot\sigma_f = 0 \text{ in } \Omega_t^f, \tag{2}$$

$$\nabla\cdot\mathbf{u}_f = 0 \text{ in } \Omega_t^f, \tag{3}$$

$$\mathbf{u}_f = \mathbf{h}_f, \text{ on } \Gamma_D^f, \quad \sigma_f\mathbf{n}_f = \mathbf{g}_f \text{ on } \Gamma_N^f \ , \ \mathbf{u}_f \circ \mathscr{A}_t = \frac{\partial \hat{\mathbf{d}}_s}{\partial t} \text{ on } \hat{\Gamma},$$

where $\left.\frac{\partial}{\partial t}\right|_{\hat{\mathbf{x}}} = \frac{\partial}{\partial t} + \mathbf{w}\cdot\nabla$ is the ALE derivative, $\mathbf{w}(\mathbf{x}) = \frac{\partial \mathscr{A}_t(\mathbf{x})}{\partial t}$ is the fluid domain velocity, $\mathbf{u}_f$ and p_f are the velocity and pressure of the fluid, respectively, and $\hat{\Gamma}$ is the common interface between the fluid and the structure on the reference configuration. We denoted by ρ_f the density of the fluid and by σ_f the Cauchy stress tensor defined for a Newtonian fluid as $\sigma_f = \mu_f(\nabla\mathbf{u}_f + (\nabla\mathbf{u}_f)^T) - p_f\mathbf{I}$, with $\mathbf{I}$ being the identity tensor, μ_f the dynamic viscosity of the fluid, and $\mathbf{n}_f$ the outward unit normal vector to $\partial\Omega_t^f$. The functions $\mathbf{h}_f$ and $\mathbf{g}_f$ indicate the Dirichlet and Neumann data applied at the Dirichlet and Neumann boundaries Γ_D^f and Γ_N^f, respectively, of Ω_t^f. Note that Γ_D^f, Γ_N^f, and Γ provide a disjoint partition of the boundary of Ω_t^f, i.e., their pairwise intersection is empty and $\bar{\Gamma}_D^f \cup \bar{\Gamma}_N^f \cup \bar{\Gamma} = \partial\Omega_t^f$. Although Γ_D^f, Γ_N^f and Γ^f depend on time t, we do not explicit it in the notation.

The structure dynamics is governed by the conservation of momentum law:

$$\hat{\rho}_s \frac{\partial^2 \hat{\mathbf{d}}_s}{\partial t^2} - \nabla_{\hat{\mathbf{x}}}\cdot\Pi(\hat{\mathbf{d}}_s) = 0 \text{ in } \hat{\Omega}^s, \tag{4}$$

$$\hat{\mathbf{d}}_s = \mathbf{h}_s \text{ on } \hat{\Gamma}_D^s, \quad \Pi(\hat{\mathbf{d}}_s)\hat{\mathbf{n}}_s = 0 \text{ on } \hat{\Gamma}_N^s \ , \quad \Pi(\hat{\mathbf{d}}_s)\hat{\mathbf{n}}_s + \hat{\sigma}_f\hat{\mathbf{n}}_f = 0 \text{ on } \hat{\Gamma}. \tag{5}$$

In Eq. (5), $\hat{\Omega}^s$ denotes the reference domain occupied by the structure (the vessel wall) at rest, $\hat{\mathbf{n}}_s$ represents the outward unit normal vector to $\partial\hat{\Omega}^s$, $\hat{\sigma}_f = (\det[\mathbf{F}])\,\mathbf{F}^{-T}\sigma_f$, $\mathbf{F} = \mathbf{I} + \nabla_{\hat{\mathbf{x}}}\hat{\mathbf{d}}_s$ is the deformation gradient tensor, and $\Pi(\hat{\mathbf{d}}_s)$ is the

first Piola–Kirchhoff stress tensor [4]. The function $\mathbf{h}_s$ indicates the Dirichlet data applied on the Dirichlet boundary $\hat{\Gamma}_D^s$ of $\hat{\Omega}^s$, $\hat{\Gamma}_N^s$ is the Neumann boundary, and $\hat{\Gamma}_D^s$, $\hat{\Gamma}_N^s$, $\hat{\Gamma}$ provide a disjoint partition of $\partial\hat{\Omega}^s$.

The coupling between the fluid, the structure and the geometry subproblems is ensured by imposing the geometry adherence, the continuity of the velocity (kinematic condition) and the continuity of the normal stresses at the interface through Equations (1), (4), and (5), respectively. We notice that the resulting system is nonlinear due to the convective term in the fluid momentum equation and to the moving fluid domain.

In Section 2 we first introduce a discretization in space and time of both the fluid problem, the structural problem and the geometry problem. In our spatial finite element discretization we allow the fluid computational grid to be non-conforming with the structural grid at the interface. Even worse, the two interfaces could be non-conforming, a situation that arises when the two subdomains are triangulated independently, for instance when dealing with an FSI problem in arterial vessels whose geometry is obtained from clinical images. A critical issue at the numerical level is the way the kinematic and dynamic coupling conditions are fulfilled. For readers' convenience we start in Section 2.1 by providing the complete algebraic formulation in the conforming case. Then, we treat in Section 2.2 the non-conforming case: after identifying a master domain (the structural domain) and a slave domain (the fluid one), we build up two RBF inter-grid operators: Π_{fs} from master to slave and Π_{sf} from slave to master. Then, we enforce the kinematic condition by equating the fluid velocity at the interface as the image through Π_{fs} of the temporal derivative of the structural displacement. On the other hand, the dynamic interface condition is fulfilled via a variational method where the *strong* form of the structural normal stress is obtained as the image through Π_{sf} of the *strong* form of the fluid normal stress. The new algebraic formulation differs very slightly from the conforming one. Section 3 is devoted to the numerical solution via a preconditioned Newton algorithm of the coupled algebraic system, while Section 4 addresses the numerical verification of our approach on an FSI problem for a straight flexible cylinder. Finally, in Section 5 we address the case of a patient–specific geometry of a femoropopliteal bypass. We discuss the computational efficiency of our method as well as its numerical accuracy.

2 Space and Time Discretizations

For space discretization, we consider a Galerkin finite element approximation using $\mathbb{P}_1$–$\mathbb{P}_1$ Lagrange polynomials for the representation of the fluid variables $\mathbf{u}_f$ and p_f, respectively, stabilized by the SUPG-ALE method [1, 2]. $\mathbb{P}_1$ finite elements are also used for the structure displacement $\hat{\mathbf{d}}_s$ and the harmonic extension $\hat{\mathbf{d}}_f$. We approximate the time derivative in the fluid momentum equation by means of the implicit Euler method. For the structure, we use a two-steps backward-difference method,

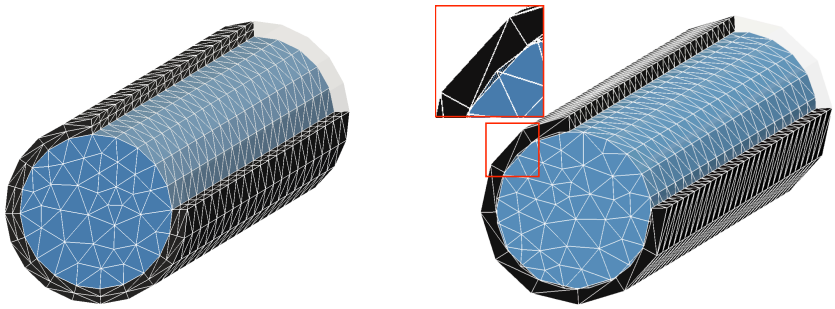

(a) Conforming meshes. (b) Non-conforming meshes.

Fig. 1: Conforming (left) and non-conforming (right) fluid–structure meshes.

$$\mathbf{d}_{n+1}^{\Delta t} - 2\mathbf{d}_{n}^{\Delta t} + \mathbf{d}_{n-1}^{\Delta t} - \hat{\rho}_s^{-1}\Delta t^2 A_s \mathbf{d}_{n+1}^{\Delta t} = 0 \tag{6}$$

where $\mathbf{d}_n^{\Delta t}$ is an approximation of of $\hat{\mathbf{d}}_s$ at time $t_n = \Delta t\, n$ and A_s is the finite element stiffness matrix associated with $-\nabla_{\hat{\mathbf{x}}} \cdot \Pi(\hat{\mathbf{d}}_s)$.

We treat the system of equations modeling the fluid-structure interaction in a monolithic fashion, i.e. we solve the FSI problem for all the unknown variables at the same time. Furthermore, we use a fully implicit scheme for which all the nonlinearities of the problem are treated implicitly.

In Sections 2.1 and 2.2 we report the fully discrete form of the nonlinear FSI system when conforming and non-conforming fluid–structure interface meshes are considered, respectively. In Fig. 1 we show an example of conforming and non-conforming fluid–structure meshes at the interface.

2.1 Conforming Fluid–Structure Interface Meshes

We assume first that at the (common) interface Γ between the fluid domain Ω_t^f and the solid domain Ω_t^s the fluid and solid meshes are the same, see Fig. 1(a). After space and time discretization, at each time step, the resulting nonlinear FSI system to be solved reads:

$$\begin{pmatrix} F(\mathbf{u}_F^{n+1}, \mathbf{d}_f^{n+1}) & 0 & I_{\Gamma^f}^T & 0 \\ 0 & S & -I_{\Gamma^s}^T & 0 \\ I_{\Gamma^f} & -I_{\Gamma^s}/\Delta t & 0 & 0 \\ 0 & -I_{\Gamma^s} & 0 & G \end{pmatrix} \begin{pmatrix} \mathbf{u}_F^{n+1} \\ \mathbf{d}_s^{n+1} \\ \lambda^{n+1} \\ \mathbf{d}_f^{n+1} \end{pmatrix} = \begin{pmatrix} \mathbf{b}_f \\ \mathbf{b}_s \\ -I_{\Gamma^s}/\Delta t\, \mathbf{d}_s^n \\ 0 \end{pmatrix}. \tag{7}$$

In Eq. (7), we denote by λ^{n+1} the vector of normal stresses (in weak form) at the fluid–structure interface and $\mathbf{u}_F^{n+1} = (\mathbf{u}_f^{n+1}, p_f^{n+1})^T$. The diagonal blocks on the left hand side of (7) account for the discretized fluid (F), structure (S) and geometry

(G) problems, respectively. We remark that F is nonlinear due to the presence of the convective term and the motion of the fluid domain. The matrices I_{Γ^f} and I_{Γ^s} are the restriction of fluid and structure vectors to the interface and account for the continuity of velocities and the geometry adherence on Γ, which are imposed strongly. Their transposes account for the continuity of the normal stresses, which is imposed weakly.

2.2 Non-conforming Fluid–Structure Interface Meshes

We consider now the case of non-conforming fluid and structure interfaces, as illustrated in Fig. 1(b). We propose a method which is able to handle both non-conforming meshes and slightly non-conforming geometries. The first case implies that the interface Γ is discretized using two different meshes depending on the side which is considered. This non-conformity is usually tackled using the mortar method [3, 9, 11]. As for the mortar method, we need to identify the so–called master and slave domains Ω_{slave} and Ω_{master}, respectively, that will play a different role. In the method proposed here, we assume the structure domain to be the master, $\hat{\Omega}^s \equiv \Omega_{master}$, while the fluid one represents the slave, $\Omega_t^f \equiv \Omega_{slave}$. In FSI problems, the normal stresses in weak form at the interface are usually computed as residuals of the fluid and structure equations. In (7) they are represented by λ. When dealing with non-conforming meshes, they have to be represented by two different vectors, λ_f on the fluid side and λ_s on the solid one.

When using non-conforming meshes, the interface coupling conditions become more involved with respect to the conforming case since an interpolation or a projection procedure has to be performed to enable the transfer of physical information between two different grids. In our method, this procedure is carried out using the Rescaled Localized Radial Basis Functions (RL-RBF) interpolant proposed in [6]. We remark that other interpolants can be used as well, however we choose RL-RBF since it allows to consider also slightly non-conforming geometries, i.e., those for which Γ^f and Γ^s do not exactly coincide.

We define the two matrices representing the interpolation between the two sides of the interface and denote them by Π_{sf}, from Γ^f to Γ^s, and Π_{fs}, from Γ^s to Γ^f. Π_{sf} needs not to be the adjoint of Π_{fs}, neither their multiplication should yield the identity matrix. In particular, this is not the case when using RL-RBF.

To better understand the way Eq. (7) is generalized to the non-conforming case, we reformulate it using the redundant variables λ_f (the normal stresses in weak form from the fluid side) and λ_s (the normal stresses in weak form from the structure side), and set $\lambda_f = \lambda_s (= \lambda)$. Then, Eq. (7) can be equivalently reformulated as:

$$\begin{pmatrix} F(\mathbf{u}_F^{n+1},\mathbf{d}_f^{n+1}) & 0 & I_{\Gamma^f}^T & 0 & 0 \\ 0 & S & 0 & -I_{\Gamma^s}^T & 0 \\ 0 & 0 & -I & I & 0 \\ I_{\Gamma^f} & -\frac{1}{\Delta t} I_{\Gamma^s} & 0 & 0 & 0 \\ 0 & -I_{\Gamma^s} & 0 & 0 & G \end{pmatrix} \begin{pmatrix} \mathbf{u}_F^{n+1} \\ \mathbf{d}_s^{n+1} \\ \lambda_f^{n+1} \\ \lambda_s^{n+1} \\ \mathbf{d}_f^{n+1} \end{pmatrix} = \begin{pmatrix} \mathbf{b}_f \\ \mathbf{b}_s \\ 0 \\ -\frac{1}{\Delta t} I_{\Gamma^s} \mathbf{d}_s^n \\ 0 \end{pmatrix}. \tag{8}$$

Here I is the identity matrix.

In the non-conforming case, the kinematic coupling condition becomes

$$\mathbf{u}_f^{n+1} = \Pi_{fs} \dot{\mathbf{d}}_s^{n+1} \quad \text{on } \Gamma^f, \tag{9}$$

which, after discretization, reads

$$\mathbf{u}_f^{n+1}|_{\Gamma^f} = \Pi_{fs} \Delta t^{-1} \left(\mathbf{d}_s^{n+1}|_{\Gamma^s} - \mathbf{d}_s^n|_{\Gamma^s} \right) \quad \text{on } \Gamma^f. \tag{10}$$

Eq. (10) replaces row 4 in Eq. (8).

We focus now on the coupling condition of the normal stresses at the fluid–structure interface. Since we are interested in interpolating quantities with the RL-RBF interpolant, we have to work with the stresses in their strong form. A simple and efficient way is to use the mass matrices of the interface on each side. In fact, denoting by λ_s^{n+1} the weak form of the normal stresses on Γ^s at time t^{n+1}, and by M_{Γ^s} and M_{Γ^f} the mass matrices associated to the structure and fluid sides of the interface, respectively, the discrete form of the dynamic coupling condition follows:

$$M_{\Gamma^s}^{-1} \lambda_s^{n+1} = \Pi_{sf} M_{\Gamma^f}^{-1} \lambda_f^{n+1} \quad \text{or} \quad \lambda_s^{n+1} - M_{\Gamma^s} \Pi_{sf} M_{\Gamma^f}^{-1} \lambda_f^{n+1} = 0 \quad \text{on } \Gamma^s. \tag{11}$$

This equation replaces row 3 in Eq. (8). In Eq. (11), we notice that $M_{\Gamma^f}^{-1} \lambda_f^{n+1}$ is an approximation of the strong form of the normal stresses on Γ^f; $\Pi_{sf}(M_{\Gamma^f}^{-1} \lambda_f^{n+1})$ is an interpolation of the normal stresses on the side of Γ^s, still in strong form, and $M_{\Gamma^s}(\Pi_{sf} M_{\Gamma^f}^{-1} \lambda_f^{n+1})$ is again in weak form but on Γ^s. Note that order of magnitude of the entries of λ_f^{n+1} depend on the mesh size used to discretize Ω_t^f, that of the entries of $M_{\Gamma^s}(\Pi_{sf} M_{\Gamma^f}^{-1} \lambda_f^{n+1})$ depend on the mesh size of $\hat{\Omega}^s$, while the order of magnitude of those of $M_{\Gamma^f}^{-1} \lambda_f^{n+1}$ and $\Pi_{sf}(M_{\Gamma^f}^{-1} \lambda_f^{n+1})$ are independent of the mesh sizes.

To summarize, in the non-conforming case Eq. (8) has to be replaced by:

$$\begin{pmatrix} F(\mathbf{u}_F^{n+1},\mathbf{d}_f^{n+1}) & 0 & I_{\Gamma^f}^T & 0 & 0 \\ 0 & S & 0 & -I_{\Gamma^s}^T & 0 \\ 0 & 0 & -\Pi_{sf} M_{\Gamma^f}^{-1} & M_{\Gamma^s}^{-1} & 0 \\ I_{\Gamma^f} & -\frac{1}{\Delta t} \Pi_{fs} I_{\Gamma^s} & 0 & 0 & 0 \\ 0 & -\Pi_{fs} I_{\Gamma^s} & 0 & 0 & G \end{pmatrix} \begin{pmatrix} \mathbf{u}_F^{n+1} \\ \mathbf{d}_s^{n+1} \\ \lambda_f^{n+1} \\ \lambda_s^{n+1} \\ \mathbf{d}_f^{n+1} \end{pmatrix} = \begin{pmatrix} \mathbf{b}_f \\ \mathbf{b}_s \\ 0 \\ -\frac{1}{\Delta t} \Pi_{fs} I_{\Gamma^s} \mathbf{d}_s^n \\ 0 \end{pmatrix}.$$

Upon eliminating λ_s^{n+1} using Eq. (11), we end up with the reduced nonlinear FSI system:

$$\begin{pmatrix} F(\mathbf{u}_F^{n+1},\mathbf{d}_f^{n+1}) & 0 & I_{\Gamma f}^T & 0 \\ 0 & S & \boxed{-I_{\Gamma s}^T M_{\Gamma s}\Pi_{sf}M_{\Gamma f}^{-1}} & 0 \\ I_{\Gamma f} & \boxed{-\frac{1}{\Delta t}\Pi_{fs}I_{\Gamma s}} & 0 & 0 \\ 0 & \boxed{-\Pi_{fs}I_{\Gamma s}} & 0 & G \end{pmatrix} \begin{pmatrix} \mathbf{u}_F^{n+1} \\ \mathbf{d}_s^{n+1} \\ \lambda_f^{n+1} \\ \mathbf{d}_f^{n+1} \end{pmatrix} = \begin{pmatrix} \mathbf{b}_f \\ \mathbf{b}_s \\ \boxed{-\frac{1}{\Delta t}\Pi_{fs}I_{\Gamma s}}\mathbf{d}_s^n \\ 0 \end{pmatrix}, \tag{12}$$

which should be regarded as the generalization of Eq. (7) to the non-conforming case. Note that we have highlighted with a box those blocks that have actually changed.

Remark: System (12) can be interpreted as the matrix representation of a finite element formulation of the FSI in the non-conforming case that generalizes the one in the conforming case by means of suitable inter-grid interface finite element operators. Full details are given in [7].

3 Numerical solution

We focus on solving Eq. (12) using the Newton method. The solution of (12) at time $t^n = n\Delta t$ is denoted by $\mathbf{X}^n = (\mathbf{u}_F^n, \mathbf{d}_s^n, \lambda_f^n, \mathbf{d}_f^n)^T$. At each time step, we compute a sequence of approximations $\mathbf{X}_1^{n+1}$, $\mathbf{X}_2^{n+1}$, etc. until the numerical solution converges up to a prescribed tolerance. The generic $k+1$ iteration of the Newton method applied to (12) is described as follows. Starting from an approximation of $\mathbf{X}_k^{n+1}$, we compute the residual $\mathbf{R}_k^{n+1} = (\mathbf{r}_{F,k}^{n+1}, \mathbf{r}_{S,k}^{n+1}, \mathbf{r}_{\lambda,k}^{n+1}, \mathbf{r}_{G,k}^{n+1})^T$:

$$\mathbf{R}_k^{n+1} = \begin{pmatrix} \mathbf{b}_f \\ \mathbf{b}_s \\ -\Pi_{fs}/\Delta t\,\mathbf{d}_s^n \\ 0 \end{pmatrix} - \begin{pmatrix} F(\mathbf{u}_F^{n+1},\mathbf{d}_f^{n+1}) & 0 & I_{\Gamma f} & 0 \\ 0 & S & -M_{\Gamma s}\Pi_{sf}M_{\Gamma f}^{-1} & 0 \\ I_{\Gamma f} & -\Pi_{fs}/\Delta t & 0 & 0 \\ 0 & \Pi_{fs} & 0 & G \end{pmatrix} \begin{pmatrix} \mathbf{u}_{F,k}^{n+1} \\ \mathbf{d}_{s,k}^{n+1} \\ \lambda_{f,k}^{n+1} \\ \mathbf{d}_{f,k}^{n+1} \end{pmatrix}.$$

Then, we compute the Newton correction $\delta\mathbf{X}_k^{n+1} = (\delta\mathbf{u}_{F,k}^{n+1}, \delta\mathbf{d}_{s,k}^{n+1}, \delta\lambda_{f,k}^{n+1}, \delta\mathbf{d}_{f,k}^{n+1})^T$ by solving

$$J_{FSI}\,\delta\mathbf{X}_k^{n+1} = -\mathbf{R}_k^{n+1}, \tag{13}$$

being J_{FSI} the exact FSI Jacobian matrix. Linear system (13) is solved by the GMRES method preconditioned by FaCSI [8]. Finally, we update the solution, i.e. $\mathbf{X}_{k+1}^{n+1} = \mathbf{X}_k^{n+1} + \delta\mathbf{X}_k^{n+1}$. We stop the Newton iterations when $\|\mathbf{R}_k^{n+1}\|_\infty / \|\mathbf{R}_0^{n+1}\|_\infty \leq \varepsilon$, being $\mathbf{R}_0^{n+1}$ the residual at the first Newton iteration and ε a given tolerance.

4 FSI in a straight flexible cylinder

In this example we consider a classical benchmark problem in which the fluid geometry consists in a straight cylinder of length $L = 5$ cm and radius $R = 0.5$ cm, surrounded by a structure of constant thickness $h = 0.1$ cm. The fluid density is $\rho_f = 1.0\ g/cm^3$, the dynamic viscosity is $\mu_f = 0.03\ g/(cm\,s)$; the structure is characterized by a density $\hat{\rho}_s = 1.2\ g/cm^3$, a Young's modulus $E_s = 3 \times 10^6\ dyne/cm^2$ and a Poisson's ratio $\nu_s = 0.3$. The structure is clamped at both ends. At the fluid inflow we prescribe a constant normal stress $\sigma \cdot \mathbf{n} = 1.33 \times 10^4\ dyne/cm^2$ for $t \leq 0.003$ s, while a homogeneous Neumann boundary conditions is used at the fluid outflow.

In our simulations we consider 3 sets of fluid–structure meshes: in Fig. 2 we report a front view of them while in Table 1 we report their corresponding number of degrees of freedom. In Fig. 3 we show a post-processing of the solutions obtained at time $t = 0.005$ s using the three different set of meshes considered. Furthermore, in Fig. 4 we compare the solutions obtained for each set by plotting the values of the pressure and the magnitude of the solid displacements with respect to time at two specific locations. In Fig. 4(b) and Fig. 4(c) we show that the results obtained using non-conforming meshes match almost exactly those obtained in the conforming case, even when the fluid mesh is much finer than the solid one (Set 3).

We also compared the performance of our solver when using the meshes of Set 1 and Set 2, for which the total number of degrees of freedom is the same. The avarage number of Newton iterations is the same and equal to 2.9, while the average number of linear solver iterations per Newton step is 20 in both cases. Finally, we observe that in the simulations performed, dealing with non-conforming meshes increases the average computational time per time step of about 15% with respect to the conforming case.

Set	Fluid DoF	Structure DoF	Coupling DoF	Geometry DoF	Total
1	137'280	53'856	13'056	102'960	307'152
2	137'280	53'856	13'056	102'960	307'152
3	840'360	53'856	48'372	630'270	1'572'858

Table 1: Straight flexible tube example: number of Degrees of Freedom (DoF) used for each set of fluid–structure meshes considered.

5 FSI in a patient–specific femoropopliteal bypass

We consider a blood flow simulation in a patient–specific femoropopliteal bypass. To estimate accurately the Wall–Shear Stress (WSS) distribution [10] we consider a fluid mesh featuring a boundary layer refinement that is non-conforming with respect to the one of the vessel wall, see Fig. 5. The blood is characterized by a

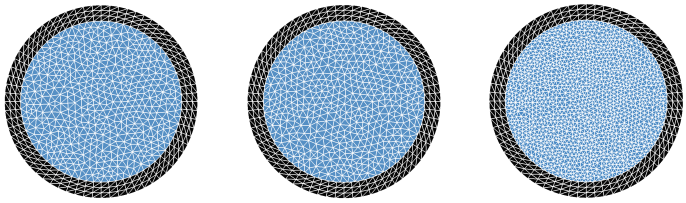

(a) Set 1. (b) Set 2. (c) Set 3.

Fig. 2: Front view of the different sets of fluid–structure meshes used. In Set 1 we consider conforming meshes. In Set 2 we keep the same meshes of Set 1 but we rotate the fluid mesh such that the fluid and structure interfaces are non-conforming. In Set 3 the structure mesh is the same of Set 1 but the fluid one is finer.

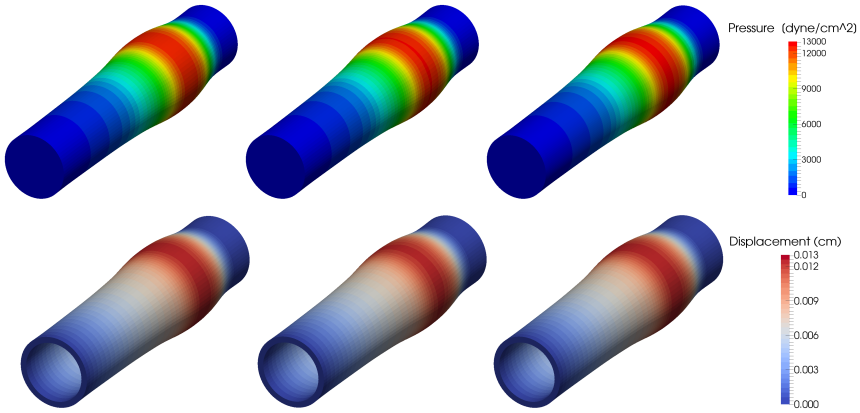

(a) Set 1. (b) Set 2. (c) Set 3.

Fig. 3: Post-processing of the results obtained at time $t = 0.005$ s. In the upper row we show the fluid pressure, while in the middle row the magnitude of the structure displacement, for the three set of meshes considered. The deformation of the fluid and structure domains is magnified by a factor 10 for visualization purposes.

density $\rho_f = 1\ g/cm^3$ and a dynamic viscosity $\mu_f = 0.0035\ g/(cm\,s)$. The Young's modulus of the vessel wall is $E_s = 4 \times 10^6\ dyne/cm^2$ and the Poisson's ratio is $\nu_s = 0.45$. Patient-specific measured inflow and outflow flow rates are imposed at the inflow and outflow sections of the fluid domain while we prescribe a homogeneous Dirichlet boundary conditions at the occluded branch. The time step considered is $\Delta t = 0.001\ s$. In Fig. 6 we show the WSS distributions computed at two different time steps during the heart-beat simulated. We notice that, although non-conforming meshes are used here, both the WSS magnitude and distribution are in good agreement with those reported in [5] where conforming fluid–structure meshes were adopted.

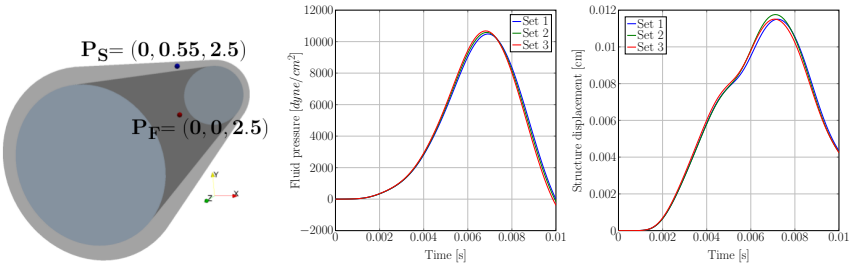

(a) Points of measure. (b) Fluid pressure at $\mathbf{P_F}$. (c) Solid displacement at $\mathbf{P_S}$.

Fig. 4: On the left we show the locations where results are taken in the fluid ($\mathbf{P_F}$) and the structure ($\mathbf{P_S}$). In the two right-most figures we report the evolution of the fluid pressure and the magnitude of the solid displacement at the point $\mathbf{P_F}$ and $\mathbf{P_S}$, respectively.

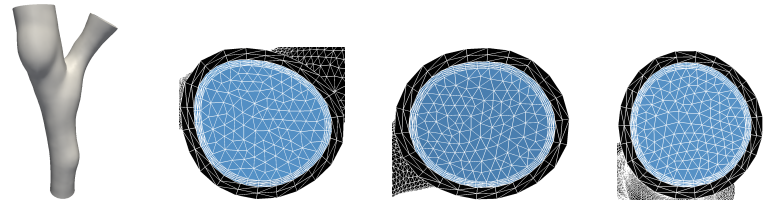

(a) Geometry. (b) Occluded branch. (c) Inflow. (d) Outflow.

Fig. 5: Bypass geometry and zoom over the inflow and outflow surfaces of the non-conforming fluid–structure meshes.

Acknowledgements The research of D. Forti was supported by the Swiss National Foundation (SNF), project No. 140184. We acknowledge Prof. P. Gervasio for the fruitful discussions and suggestions. We gratefully acknowledge the Swiss National Supercomputing Centre (CSCS) for providing us the CPU resources under project ID s475. We also thank the LifeV community.

References

1. Y. Bazilevs, V. M. Calo, J. A. Cottrell, T. J. R. Hughes, A. Reali, and G. Scovazzi: Variational multiscale residual–based turbulence modeling for large eddy simulation of incompressible flows. Comput. Methods Appl. Mech. Engrg. **197**(1-4), 173–201 (2007).
2. Y. Bazilevs, K. Takizawa, and T.E. Tezduyar: Computational Fluid–Structure Interaction. Methods and Applications. Wiley Series in Computational Mechanics. Wiley (2013).
3. C. Bernardi, Y. Maday, A. T. Patera: A new nonconforming approach to domain decomposition: the mortar element method. In: Brezis, H., Lions, J. L., (eds.) Nonlinear Partial Differential Equations and their Applications, pp. 13-51. Pitman Wiley, London/New York (1994).

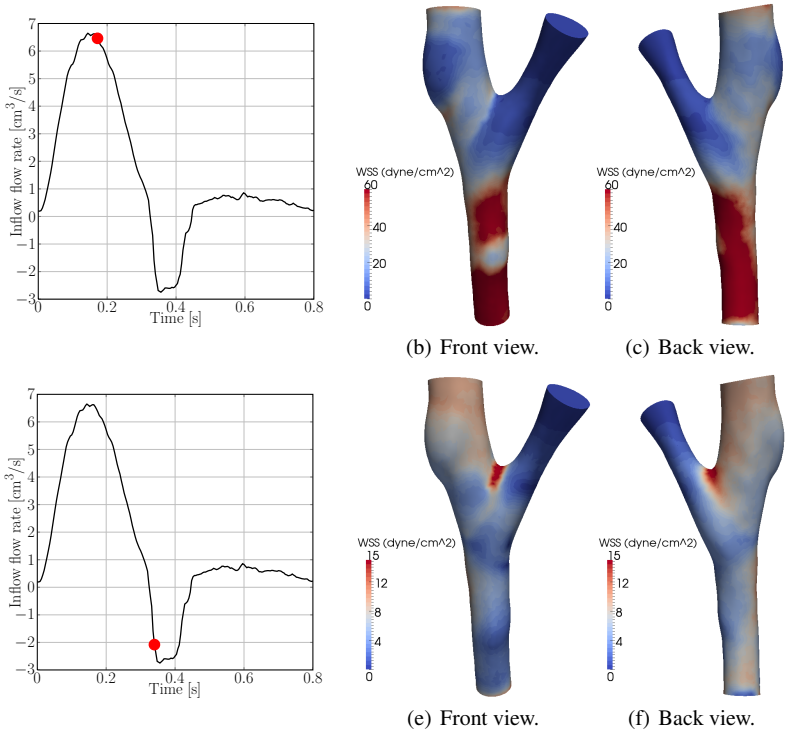

(b) Front view. (c) Back view.

(e) Front view. (f) Back view.

Fig. 6: WSS distributions at times $t = 0.17\ s$ (top) and at $t = 0.34\ s$ (bottom).

4. P. Crosetto, S. Deparis, G. Fourestey, and A. Quarteroni: Parallel algorithms for fluid-structure interaction problems in haemodynamics. SIAM J. Sci. Comput. **33**(4), 1598-1622 (2011).
5. C. Colciago, S. Deparis, and A. Quarteroni: Comparisons between reduced order models and full 3D models for fluid-structure interaction problems in haemodynamics. J. Comput. Appl. Math. **265**, 120-138 (2014).
6. S. Deparis, D. Forti, and A. Quarteroni: A Rescaled Localized Radial Basis Function Interpolation on Non-Cartesian and Nonconforming Grids. SIAM J. Sci. Comput. **36**(6), A2745-A2762 (2014). (2011).
7. S. Deparis, D. Forti, P. Gervasio, and A. Quarteroni: An accurate interpolation based method for non–conforming interfaces. In preparation (2015).
8. S. Deparis, D. Forti, G. Grandperrin, and A. Quarteroni: FaCSI: A block parallel preconditioner for fluid-structure interaction in hemodynamics. Submitted (2015).
9. T. Klöppel, A. Popp, U. Küttler, and W. A. Wall: Fluid–structure interaction for non–conforming interfaces based on a dual mortar formulation. Comput. Methods Appl. Mech. Engrg. **200**, 3111-3126 (2011).
10. E. Marchandise, P. Crosetto, C. Geuzaine, J.-F. Remacle, and E. Sauvage: Quality open source mesh generation for cardiovascular flow simulations. In: Ambrosi, D., Quarteroni, A., Rozza, G., (eds.) Modeling of Physiological Flows, pp. 395-414. Springer, Milan (2012).
11. B. I. Wohlmuth: A mortar finite element method using dual spaces for the Lagrange multiplier. SIAM J. Numer. Anal. **38**(3) 989-1012 (2000).

Recent publications:

MATHEMATICS INSTITUTE OF COMPUTATIONAL SCIENCE AND ENGINEERING
Section of Mathematics
Ecole Polytechnique Fédérale
CH-1015 Lausanne

04.2015 FABIO NOBILE, LORENZO TAMELLINI, FRANCESCO TESEI, RAÚL TEMPONE:
An adaptive sparse grid alorithm for elliptic PDEs with lognormal diffusion coefficent

05.2015 MICHAEL STEINLECHNER:
Riemannian optimization for high-dimensional tensor completion

06.2015 V. R. KOSTIĆ, A. MIEDLAR, LJ. CVETKOVIĆ:
An algorithm for computing minimal Geršgorin sets

07.2015 ANDREA BARTEZZAGHI, LUCA DEDÈ, ALFIO QUARTERONI:
Isogeometric analysis of high order partial differential equations on surfaces

08.2015 IVAN FUMAGALLI, ANDREA MANZONI, NICOLA PAROLINI, MARCO VERANI:
Reduced basis approximation and a posteriori error estimates for parametrized elliptic eigenvalue problems

09.2015 DAVIDE FORTI, LUCA DEDÈ:
Semi-implicit BDF time discretization of the Navier-Stokes equations with VMS-LES modeling in a High Performance Computing framework

10.2015 PETAR SIRKOVIĆ, DANIEL KRESSNER:
Subspace acceleration for large-scale parameter-dependent Hermitian eigenproblems

11.2015 FEDERICO NEGRI:
A model order reduction framework for parametrized nonlinear PDE-constrained optimization

12.2015 ANNA TAGLIABUE, LUCA DEDÈ. ALFIO QUARTERONI:
Nitsche's method for parabolic partial differential equations with mixed time varying boundary conditions

13.2015 SIMONE DEPARIS, DAVIDE FORTI, GWENOL GRANDPERRIN, ALFIO QUARTERONI:
FaCSI: A block parallel preconditioner for fluid-structure interaction in hemodynamics

14.2015 ASSYR ABDULLE, TIMOTHÉE POUCHON:
A priori error analysis of the finite element heterogenenous multiscale method for the wave equation in heterogenenous media over long time

15.2015 ANDREA MANZONI, STEFANO PAGANI:
A certified reduced basis method for PDE-constrained parametric optimization problems by an adjoint-based approach

16.2015 SIMONE DEPARIS, DAVIDE FORTI, ALFIO QUARTERONI:
A fluid-structure interaction algorithm using radial basis function interpolation between non-conforming interfaces